ACS APPLIED MATERIALS & INTERFACES

Research Article

www.acsami.org

Novel Coupled Structures of $FeWO_4/TiO_2$ and $FeWO_4/TiO_2/CdS$ Designed for Highly Efficient Visible-Light Photocatalysis

Sandipan Bera,[†] Sher Bahadur Rawal,[†] Hark Jin Kim, and Wan In Lee*

Department of Chemistry and Chemical Engineering, Inha University, Incheon 402-751, Korea

ABSTRACT: A quadrilateral disk-shaped $FeWO_4$ nanocrystal (NC) with an average size of ~35 nm was prepared via hydrothermal reaction. The obtained dark brown $FeWO_4$ NC with a bandgap (E_g) of 1.98 eV was then coupled with TiO_2 to form $FeWO_4/TiO_2$ composites. The valence band (VB) of $FeWO_4$ (+2.8 eV vs NHE) was more positive than that of TiO_2 (+2.7 eV); thus this system could be classified as a Type-B heterojunction. Under visible-light irradiation, 5/95 $FeWO_4/TiO_2$ (by wt %) exhibited remarkable photocatalytic activity: the amount of CO_2 evolved from gaseous 2-propanol (IP) and the decomposition rate of aqueous salicylic acid (SA) were, respectively, 1.7 and 2.5 times greater than those of typical nitrogen-doped TiO_2 (N-TiO_2). This unique catalytic property was deduced to arise from the intersemiconductor hole transfer between the VBs of $FeWO_4$ and TiO_2. Herein, several experimental evidence were also provided to confirm the hole-transfer mechanism. To further enhance the catalytic efficiency, double-heterojunctioned $FeWO_4/TiO_2/CdS$ composites were prepared by loading CdS quantum dots (QDs) onto the $FeWO_4/TiO_2$ surface. Surprisingly, the catalytic activity for evolving CO_2 from IP was 2.6 times greater than that of bare $FeWO_4/TiO_2$ and 4.4 times greater than that of N-TiO_2, suggesting that both holes and electrons were essential species in decomposing organic compounds.

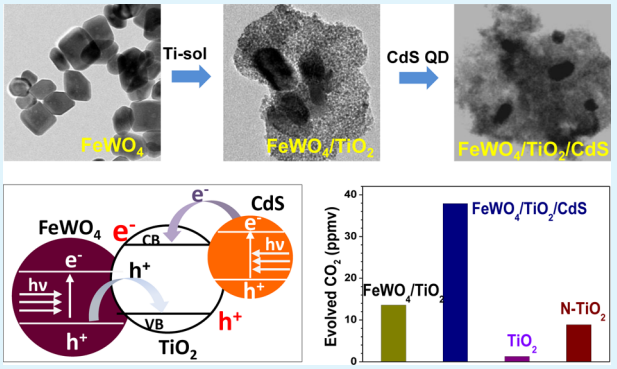

KEYWORDS: *photocatalyst, $FeWO_4/TiO_2$, heterojunction, visible-light, organic pollutant, hole transfer*

INTRODUCTION

The removal of organic contaminants via photocatalytic processes has been recognized as a potential strategy for treating environmental pollutions in air and water. TiO_2 has been known to be the most efficient photocatalyst among various semiconductors, because of its unique characteristics in band position and surface structure, as well as its high electron mobility, chemical stability, and nontoxicity.[1−6] Because of its large bandgap (E_g = 3.2 eV), however, TiO_2 is only functional in the UV region, occupying less than 4% of the solar spectrum.[7−11] Thus, designing novel photocatalysts that can utilize visible light is prerequisite in enhancing photocatalytic efficiency and extending the range of applications.

Major strategies for designing visible-light photocatalysts include modifying or narrowing the TiO_2 E_g by doping cations such as Cr, Fe, Ni, or V ions,[12−17] to Ti sites and/or by doping anions such as N, S, C, or B,[18−22] to O sites. Another notable approach involves combining narrow E_g semiconductors or molecular sensitizers with the TiO_2.[23−28,32−38]

Two types of heterojunctions can be designed for the visible-light photocatalysis, depending on the location of the relative energy band between the narrow E_g semiconductors and TiO_2. First, the conduction band (CB) of the visible-light sensitizer is more negative than that of TiO_2 (which is classified as a Type-A heterojunction). For example, several metal chalcogenide quantum dots (QDs) or molecular dyes are loaded on the TiO_2 surface to form Type-A heterojunctions.[24−28] With visible-light irradiation to this system, the sensitizer is excited, and the electrons are then transported to the TiO_2 CB. These electrons can induce reduction reactions or participate in oxidation reactions by forming $\bullet O_2^-$ and $HO_2\bullet$, as shown in eqs 1−3.[29,30]

$$O_2 + e^- \rightarrow \bullet O_2^- \qquad E_0 = -0.284\ \text{V (vs NHE)} \tag{1}$$

$$\bullet O_2^- + H^+ \rightarrow HO_2\bullet \qquad E_0 = -0.046\ \text{V (vs NHE)} \tag{2}$$

$$HO_2\bullet + \text{organic compounds} \rightarrow \rightarrow \rightarrow CO_2 + H_2O \tag{3}$$

Second, the valence band (VB) of the sensitizer is more positive than that of TiO_2 (which is classified as a Type-B heterojunction). With the irradiation of visible light to this coupled system, the electrons in the sensitizer VB are excited to its CB. Thereby, the holes in the sensitizer VB can be transferred to that of TiO_2, as shown in Scheme 1a. Consequently, holes are generated in the TiO_2 VB by an intersemiconductor hole-transfer mechanism, which, in turn, initiate oxidation reactions by generating $\bullet$OH radicals on the TiO_2 surface, as shown in eqs 4 and 5.[31]

Received: April 5, 2014
Accepted: May 21, 2014
Published: May 21, 2014

   dx.doi.org/10.1021/am502079x | *ACS Appl. Mater. Interfaces* 2014, 6, 9654−9663

Scheme 1. Diagram for Charge Flows Occurring in (a) $FeWO_4/TiO_2$ and (b) Double-Heterojunctioned $FeWO_4/TiO_2/CdS$ Composites upon Visible-Light Irradiation; (c) Schematic Diagram of the Preparation Strategy for the $FeWO_4/TiO_2/CdS$ Composite

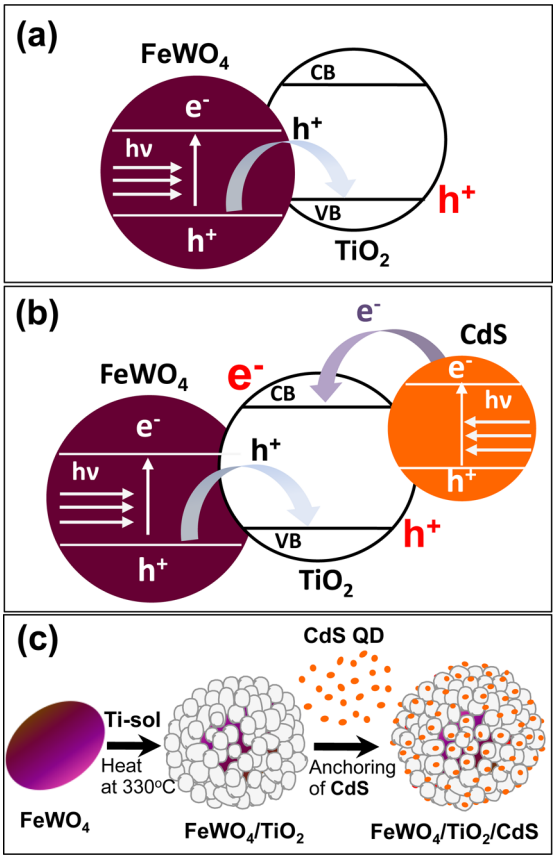

$$(H_2O)_{ads} + h^+ \rightarrow H^+ + \bullet OH \quad (4)$$

$$(OH^-)_{ads} + h^+ \rightarrow \bullet OH \quad (5)$$

The holes created in the TiO_2 VB are more powerful than the $\bullet O_2^-$ or $HO_2\bullet$ in oxidizing organic compounds. Thus, Type-B heterojunction systems are considered to be more efficient than Type-A systems for completely decomposing organic pollutants, as discussed by Rawal et al.[32] Thus, far several Type-B heterojunction structures such as WO_3/TiO_2,[33] $FeTiO_3/TiO_2$,[34] Bi_2O_3/TiO_2,[35] Sb-doped SnO_2/TiO_2,[36] Ag_3PO_4/TiO_2,[37] and $W_{18}O_{49}/TiO_2$,[38] have been reported to exhibit significant visible-light photocatalytic activities, and some of them demonstrate catalytic activity comparable to that of nitrogen-doped TiO_2 (N-TiO_2).

In designing efficient visible-light photocatalysts based on Type-B heterojunction structures, the following properties are required for narrow E_g semiconductors (sensitizers):

(a) The VB level of sensitizers must be more positive than that of TiO_2 for efficient hole transport.
(b) A small E_g and a high molar absorption coefficient are necessary for the efficient utilization of visible light.
(c) The inherent hole-diffusion coefficient should be high with a low charge recombination rate.
(d) The CB level of the sensitizer should be sufficiently high that the accumulated electrons in the CB can be effectively scavenged.

Considering the CB level of sensitizer, direct electron transfer to the oxygen molecules, as shown in eqs 1 and 2, will be difficult. Thus, the electrons in the sensitizer CB might be transported to the oxygen species via multielectron processes shown in eqs 6 and 7, suggesting that the sensitizer CB level must at least be higher than +0.682 or +1.23 V (vs NHE).[39,40]

$$O_2 + 2H^+ + 2e^- \rightarrow H_2O_2 \qquad E_0 = +0.682\ V \quad (6)$$

$$O_2 + 4H^+ + 4e^- \rightarrow 2H_2O \qquad E_0 = +1.23\ V \quad (7)$$

Herein, we report a novel $FeWO_4/TiO_2$ system that exhibits significantly higher visible-light photocatalytic efficiency than N-TiO_2. $FeWO_4$ belongs to the wolframite-type family, which has potential applications in scintillation detectors, optical fibers, humidity sensors, photoanodes, optical devices, catalysts, and pigments.[41,42] Thus far, however, $FeWO_4$ has not been applied to fabricate visible-light photocatalytic systems. In the literature, the E_g of $FeWO_4$ is reported to be in the range of 1.78−2.35 eV,[43−46] depending on the particle morphology and the measurement method. In this work, ∼35-nm-sized $FeWO_4$ NC was prepared via the hydrothermal method. Its E_g was determined to be 1.98 eV, while the VB level is significantly more positive than that of TiO_2. Moreover, it exhibits profound absorption in the visible-light range and extensive chemical and thermal stability, thereby satisfying most of the requirements for a sensitizer in designing efficient visible-light photocatalyst. Hole transport from $FeWO_4$ to TiO_2 is considered to be the main catalytic mechanism in this system, and several pieces of evidence have been provided to support this mechanism. To enhance the photocatalytic activity further, a double heterojunction structure of $FeWO_4/TiO_2/CdS$ was fabricated and its catalytic mechanism (Scheme 1b) was also discussed.

EXPERIMENTAL METHODS

Synthesis of $FeWO_4$ NC. Two millimoles (2 mmol) of sodium tungstate ($Na_2WO_4{\cdot}2H_2O$, Aldrich) and 2 mmol of ferrous ammonium sulfate [$(NH_4)_2Fe(SO_4)_2{\cdot}6H_2O$, Aldrich] were dissolved in 25 mL of distilled water in separate beakers. The ferrous ammonium sulfate solution was then added to the sodium tungstate solution dropwise, accompanied by vigorous stirring. The solution was stabilized by adjusting the pH to 8 by adding aqueous NaOH solution. The entire mixture was then transferred to a 100 mL Teflon-lined autoclave and reacted at 180 °C for 12 h. The resulting dark brown-colored precipitate was washed several times with a water/ethanol mixture and dried at 80 °C for 12 h.

Synthesis of $FeWO_4/TiO_2$ Composites and Other Catalytic Materials. A quantity of 3.67 g of titanium isopropoxide (97%, Aldrich) was stabilized in a mixed solution of 40 mL of ethanol, 1.0 mL of concentrated nitric acid, and 1.0 mL of water. Then, the prepared Ti-precursor solution was gently stirred for 4 h. A stoichiometric amount of the as-prepared $FeWO_4$ was then added to this solution. Typically, the 5/95 $FeWO_4/TiO_2$ composite (5 wt % $FeWO_4$ and 95 wt % TiO_2) was obtained by adding 53 mg of $FeWO_4$ NC presuspended in 10 mL of ethanol to the prepared Ti-precursor solution, which was gently stirred overnight. The resulting mixture was completely dried at 80 °C for 24 h. The obtained powder was resuspended in 50 mL of ethanol in a closed vessel and then stirred for 24 h on a hot plate kept at 110 °C. This aging process facilitated the conversion of amorphous titania to the anatase phase. The suspension was then centrifuged, dried, and subsequently heat-treated at 330 °C for 5 h. Bare TiO_2 was prepared as a blank sample by the same procedure without adding $FeWO_4$ NC. A typical N-TiO_2 sample was used as a standard to compare the visible-light activity of various photocatalytic materials. The N-TiO_2 sample was prepared by flowing NH_3 gas (flow rate: 0.07 L min^{-1}) over 1.0 g of Degussa P25 at 550 °C for 3 h.[47]

dx.doi.org/10.1021/am502079x | ACS Appl. Mater. Interfaces 2014, 6, 9654−9663

Synthesis of CdS and Surface Modification. Cadmium sulfide (CdS) quantum dots (QDs) were synthesized in octadecene (ODE, Aldrich) by adding oleic acid as a capping agent. The procedure consisted of mixing 0.0128 g of CdO, 0.113 g of oleic acid, and 1.51 g of ODE in a three-necked flask and heating the mixture to 300 °C under an anhydrous N_2 flow. A solution containing 0.0016 g of sulfur and 2.36 g of ODE in a beaker was quickly injected into the heated solution. The temperature of the mixture was then adjusted to 260 °C to induce the growth of CdS. After 10 min, the reaction was quenched by adding 30 mL of cold toluene. Fifty milliliters (50 mL) of an ethanol/chloroform mixture was added to the entire reaction mixture to extract the unreacted reactants or impurities, and finally, 30 mL of acetone was added to the remaining solution to precipitate the oleic acid-capped CdS.

To attach CdS QD to the TiO_2 surface, the oleic acid on the surface of CdS QD was exchanged for the mercaptopropionate group, following a procedure reported by Leschkies et al.[48] Next, 0.2 mmol of mercaptopropionic acid (MPA, Aldrich) was dissolved in 100 mL of anhydrous methanol, and the pH of the resulting solution was adjusted to 11.4 by adding tetramethylammonium hydroxide (TMAH, Aldrich). Forty milligrams (40 mg) of oleic acid-capped CdS was then added to this solution. The mixture was heated to 63 °C under an argon atmosphere and refluxed for 24 h in darkness. The formed MPA-capped CdS QD was precipitated by adding a 1:1 mixture of ethyl acetate and diethyl ether. The collected precipitate was washed several times with ethyl acetate to remove residual MPA or oleic acid. The prepared CdS QD was then readily soluble in protic solvents.

Preparation of $FeWO_4/TiO_2$/CdS Composites. A stoichiometric amount of the MPA-capped CdS was added to a 50-mL ethanol suspension containing 1.00 g of the 5/95 $FeWO_4/TiO_2$ composite, and the resulting solution was stirred vigorously at 60 °C for 6 h. The 1 wt % CdS loaded $FeWO_4/TiO_2$ composite was prepared by adding 10.1 mg of MPA-capped CdS (see Scheme 1c). During the stirring, the MPA-capped CdS QD was bound to the TiO_2 in $FeWO_4/TiO_2$. The resulting $FeWO_4/TiO_2$/CdS composite was then precipitated by centrifugation, and the collected sample was heated at 200 °C for 2 h to facilitate tight binding.

Characterizations. X-ray diffraction (XRD) patterns of the prepared photocatalytic samples were obtained using a Rigaku Multiflex diffractometer with monochromatic Cu Kα radiation. XRD scanning was performed under ambient conditions over a 2θ region of 20°–60° at a rate of 2 °/min (40 kV, 20 mA). UV visible diffuse reflectance spectra were acquired using a Perkin–Elmer Model Lambda 40 spectrophotometer. $BaSO_4$ was used as the reflectance standard. Transmission electron microscopy (TEM) and EDX elemental mapping images were obtained using a JEOL Model JEM2100F operated at 200 kV. Brunauer–Emmett–Teller (BET) surface areas of the samples were measured using a surface area and porosimetry analyzer (UPA-150, Microtrac, Inc.). The flat-band potentials (V_{fb}) of $FeWO_4$ and TiO_2 were determined using the Mott–Schottky method.[49] Each powdered sample was coated as a film on a 1 cm × 1 cm Pt-coated Pyrex glass. The flat-band potential of each semiconductor was determined by extrapolating the plot of the inverse square of the capacitance ($1/C_{sc}^2$) versus the applied potential (V) for 0.2 M $LiClO_4$ in acetonitrile. Ag/AgCl and Pt were used as the reference and the counter electrode, respectively.

Evaluation of Photocatalytic Activity. First, the visible-light photocatalytic activities of the samples were estimated by monitoring the decomposition of gaseous 2-propanol (IP). An aqueous suspension containing 8.0 mg of the photocatalytic samples was spread on a 2.5 cm × 2.5 cm Pyrex glass as a film and subsequently dried at room temperature. Prior to the photocatalytic measurement, the prepared film was irradiated by a 300 W Xe lamp for 3 h, to remove potential organic residues. The net volume of the gas-tight reactor was 200 mL, and the photocatalytic film was located at the center of the reactor. The entire area of the photocatalytic film was irradiated by a 300 W Xe lamp that was installed with a UV cutoff filter ($\lambda \geq 420$ nm, Oriel) and a water filter to cutoff the IR spectrum. After the reactor was evacuated, 1.6 mL of the water-diluted IP (IP:H_2O = 1:9 in volume) was injected into the reactor. The initial concentration of gaseous IP in the reactor was maintained at 117 ppm by volume (ppmv). Thus, the ultimate concentration of CO_2 evolved, after complete decomposition of the IP, should have been 351 ppmv, as shown by the following equation:

$$2(CH_3)_2CHOH(g) + 9O_2(g) = 6CO_2(g) + 8H_2O(g) \quad (8)$$

The total pressure of the reactor was then increased to 750 Torr by adding oxygen gas. Under these conditions, the IP and H_2O remained in the vapor phase. For every 30 min of irradiation, 0.5 mL of the gas in the reactor was collected and sent to a gas chromatograph (Agilent Technologies, Model 6890N) using an auto sampling valve system. A methanizer was installed between the gas chromatography (GC) column outlet and the flame ionization detection (FID) device for CO_2 detection.

Second, for the photocatalytic degradation of salicylic acid (SA) in aqueous solution, 10 mg $FeWO_4/TiO_2$ of composites or other photocatalytic samples were suspended in 50 mL of a 50 μM SA aqueous solution. After the irradiation of visible light, the residual SA was identified by its characteristic absorption peak using an ultraviolet–visible light (UV-vis) spectrophotometer (Perkin–Elmer, Model Lambda 40).

RESULTS AND DISCUSSION

$FeWO_4$ NC was prepared by a hydrothermal reaction under a basic condition at 180 °C for 12 h. Figure 1 shows the XRD

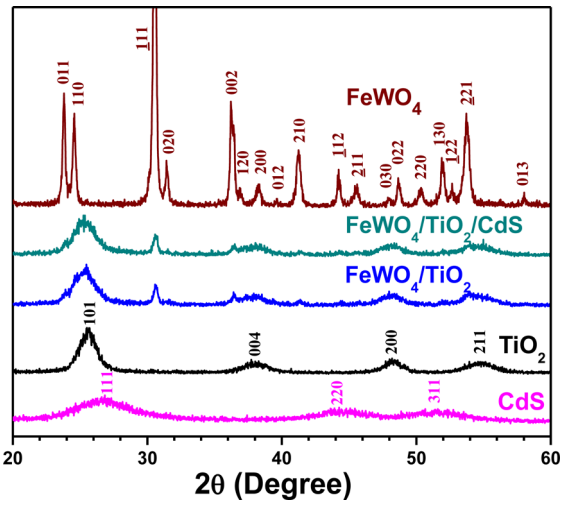

Figure 1. XRD patterns of several powder samples. Ratio of $FeWO_4$:TiO_2 in $FeWO_4/TiO_2$ was 5:95 (based on wt %), and the loaded amount of CdS was 1 wt % in the $FeWO_4/TiO_2$/CdS composite.

patterns of the as-prepared $FeWO_4$ NC in the highly crystallized monoclinic phase (JCPDS File Card No. 21-0436) in which there were no noticeable impurity phases. The average crystallite size of the as-prepared $FeWO_4$ NC, determined from the (011) and (110) peaks by applying the Scherrer equation, was ~30 nm.

The TEM images in Figure 2 show that the as-prepared $FeWO_4$ NC had a quadrilateral disk-type structure that was ~35 nm in size. The individual NCs were separated from each other, and no heavy agglomeration was observed. The dashed square in Figure 2b is magnified in Figure 2c. The spacing of the fringe patterns was measured to be 0.473 nm, corresponding to d_{100} of the monoclinic $FeWO_4$ phase. Selected-area electron diffraction (SAED) patterns were also monitored over the entire area of a single particle, as shown in Figure 2b. The uniformly aligned spot patterns in Figure 2d

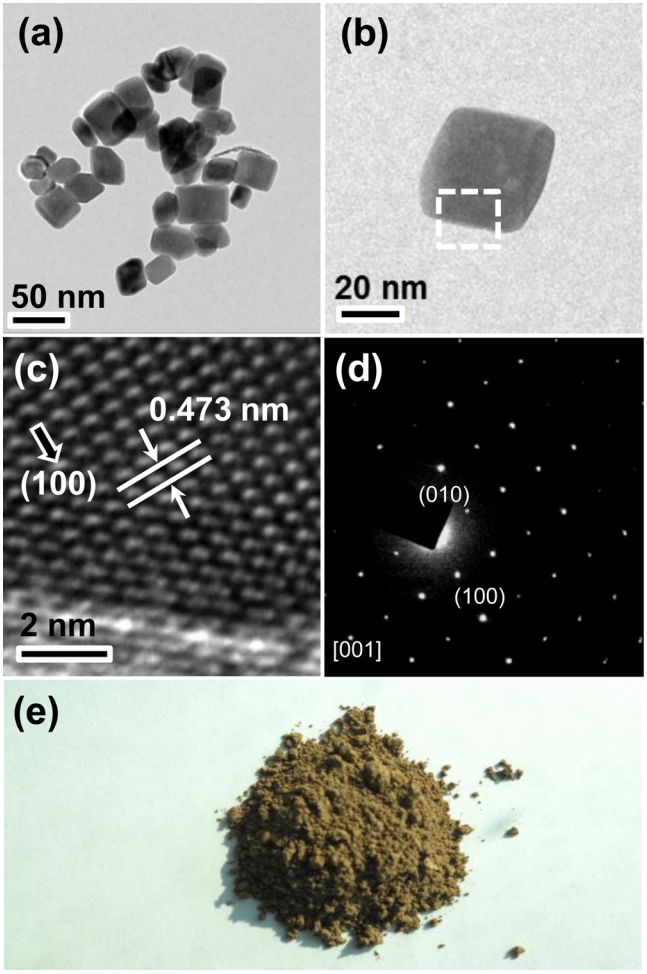

Figure 2. TEM image of (a) as-prepared $FeWO_4$ NC, (b) magnified image for a single particle, and (c) high-resolution image for dashed square in panel b. (d) SAED patterns obtained from single $FeWO_4$ NC shown in panel b, and (e) photographic image of the as-prepared $FeWO_4$ NC.

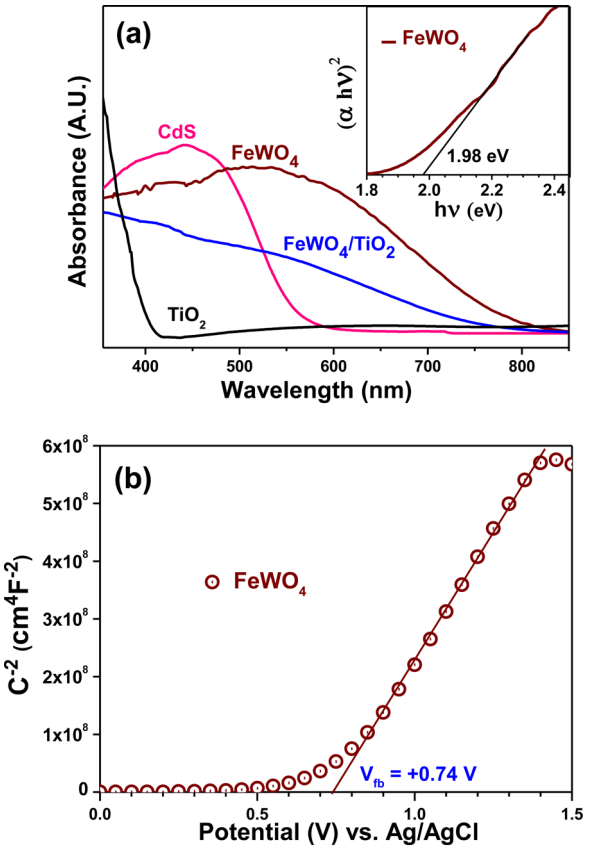

Figure 3. (a) UV-vis absorbance spectra of several powder samples acquired in reflection mode. Kubelka–Munk (KM) plot of the $FeWO_4$ NC is included in the inset. (b) Mott–Schottky plot of $FeWO_4$. Active area of semiconductor films deposited on Pt/Pyrex was 1 cm^2, and 0.2 M $LiClO_4$ in acetonitrile was used as an electrolyte. Pt wire was used as the counter electrode, and the saturated Ag/AgCl was used as the reference electrode.

confirmed that the individual $FeWO_4$ NCs were a single crystal in the monoclinic phase.

As shown in Figure 2e, the as-prepared $FeWO_4$ is dark brown in color, suggesting that it can absorb a considerable portion of visible light. Figure 3a shows the UV-vis diffuse reflectance spectrum of $FeWO_4$ that was obtained in absorption mode, indicating that the $FeWO_4$ NC exhibit profound absorption over the entire visible region. The direct E_g of $FeWO_4$ NC was estimated by the Kubelka–Munk (KM) plot, as shown in the inset of Figure 3a. The E_g of the $FeWO_4$ NC was determined to 1.98 eV, which was quite close to the reported value of 2.0 eV.[50] The V_{fb} value of the $FeWO_4$ NC, which is considered to be an *n*-type semiconductor, was obtained using a Mott–Schottky plot (see Figure 3b). The CB of $FeWO_4$ was +0.82 V (vs NHE). Using the E_g of $FeWO_4$ of 1.98 eV, the VB level was then estimated to be +2.80 V (vs NHE), suggesting that the $FeWO_4$ VB was more positive than the TiO_2 VB, which is known to be +2.70 V (vs NHE).

The $FeWO_4/TiO_2$ composites were prepared by using a sol–gel method to cover the relatively large $FeWO_4$ NC with TiO_2, as described in Scheme 1c. The X-ray diffraction (XRD) patterns of 5/95 $FeWO_4/TiO_2$ (5 wt % $FeWO_4$ and 95 w% TiO_2) and blank TiO_2 are also included in Figure 1. The blank TiO_2, prepared by calcining the sol–gel processed Ti-precursor at 330 °C, exhibits a pure anatase phase. Its crystallite size was determined to be ~7 nm by applying the Scherrer equation. The TEM images in Figures 4a and 4b show the 5/95 $FeWO_4/TiO_2$. A few $FeWO_4$ NCs were embedded in the sol–gel-derived TiO_2. Figure 4c is a high-magnification image describing the interface between TiO_2 and $FeWO_4$, showing that the sol–gel derived TiO_2 is tightly bound to the $FeWO_4$ NC. The dashed square in Figure 4c is magnified in Figure 4d to analyze the fringe patterns. The spacing of 0.352 nm was identified as the (101) plane of the anatase TiO_2 phase, indicating that the sol–gel-derived TiO_2 covering the $FeWO_4$ NC had a polycrystalline structure.

The photocatalytic activities of several composites were evaluated by monitoring the decomposition of gaseous 2-propanol (IP) under visible-light irradiation ($\lambda \geq 420$ nm). By photocatalytic reaction, the gaseous IP is initially oxidized to acetone, and ultimately mineralized to CO_2. The decomposition reaction of IP was approximated to the first-order kinetics. Hence, the photocatalytic reaction can be described by $-d[c]/dt = k[c]$, where $[c]$ is the IP concentration, and k denotes the degradation rate constant. Figure 5a shows the removal of IP as a function of visible-light irradiation time in the presence of several photocatalytic samples. Table 1 lists the determined degradation rate constants (k_{IP}) and those per unit area (k_{IP}/A, where A is the surface area of the catalyst) in

dx.doi.org/10.1021/am502079x | ACS Appl. Mater. Interfaces 2014, 6, 9654–9663

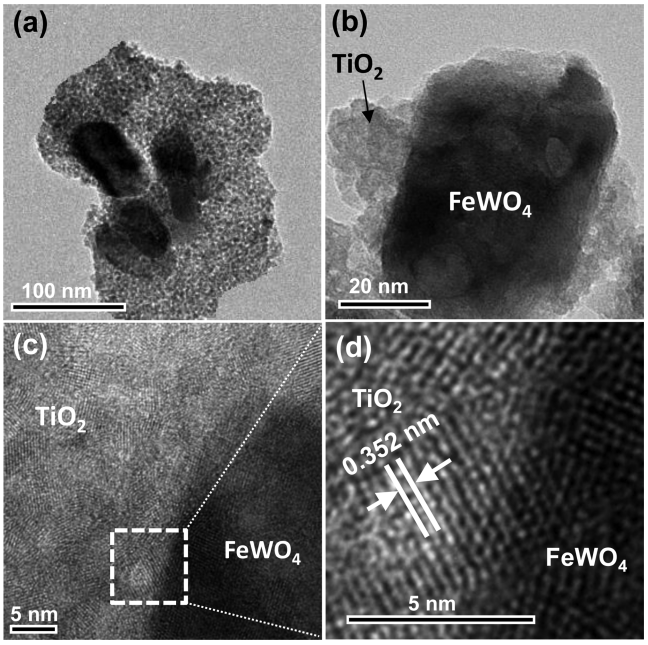

Figure 4. (a, b) TEM images of 5/95 $FeWO_4/TiO_2$ composite, (c) corresponding high-resolution image, and (d) magnified image of dashed square in panel c.

decomposing IP with several photocatalytic samples. The $FeWO_4/TiO_2$ composites exhibited remarkably higher k_{IP} values than bare $FeWO_4$ or blank TiO_2, and the 5/95 $FeWO_4/TiO_2$ exhibited the highest efficiency among the composites in various compositions: the k_{IP} value of the 5/95 $FeWO_4/TiO_2$ was 39 and 63 times greater than that of the bare $FeWO_4$ and TiO_2, respectively. Furthermore, the k_{IP} of 5/95 $FeWO_4/TiO_2$ was 6.2 times that of N-TiO_2. In 2 h, ~90% IP was removed by 5/95 $FeWO_4/TiO_2$, whereas only 34% was removed by N-TiO_2.

The photocatalytic activity was also evaluated by monitoring the CO_2 evolution under visible-light irradiation. As shown in Figure 5b, the $FeWO_4/TiO_2$ composites also exhibit the greatly enhanced efficiencies in CO_2 evolution. The optimal efficiency was obtained from the 5/95 $FeWO_4/TiO_2$ composite: 14.7 ppmv of CO_2 was evolved in 2 h, whereas 8.7 ppm was evolved using N-TiO_2.

Figure 5c shows the photocatalytic activities for several catalytic systems in decomposing SA in aqueous solution under visible-light irradiation. As in the gaseous IP decomposition, the 5/95 $FeWO_4/TiO_2$ exhibited the highest photocatalytic activity of all the systems. The rate constant for SA decomposition was ~15 times higher than that of bare $FeWO_4$ or TiO_2. The detailed results are given in Table 1. The surface areas of the $FeWO_4/TiO_2$ composites decreased somewhat as the composition of $FeWO_4$ in the composite increased, indicating that the surface area was not a crucial factor in determining the catalytic activity of the $FeWO_4/TiO_2$ composites.

It is deduced that the remarkably high photocatalytic activity of $FeWO_4/TiO_2$ was primarily caused by the unique energy band location of $FeWO_4$. The VB level of $FeWO_4$ (+2.80 V vs NHE) was found to be more positive than that of TiO_2 (+2.70 V vs NHE). Under visible-light irradiation, the electrons in the VB of $FeWO_4$ are excited to its CB. Then, the holes in the $FeWO_4$ VB could be transferred to the TiO_2 VB, as shown in Scheme 1a. This intersemiconductor hole-transport process

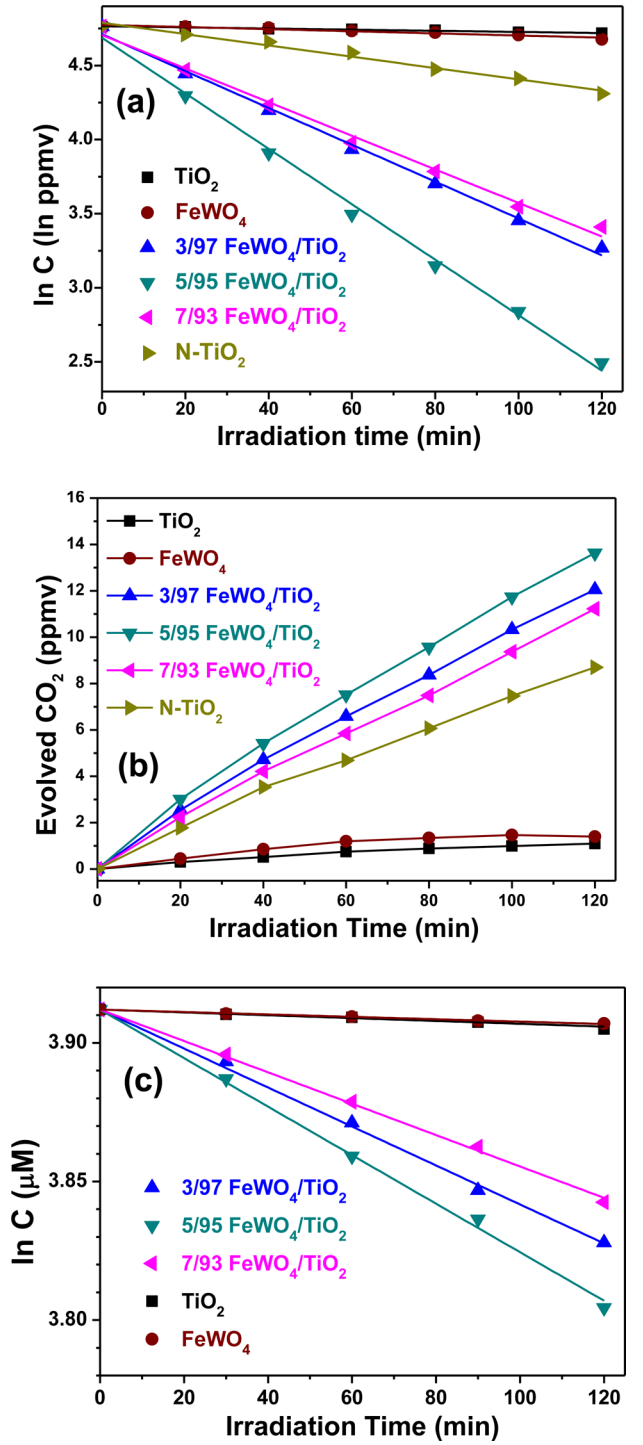

Figure 5. (a) Remnant IP concentration, and (b) amounts of CO_2 evolved as a function of irradiation time in the photocatalytic decomposition of gaseous IP under visible-light irradiation ($\lambda \geq 420$ nm). (c) Remnant SA concentration as a function of irradiation time in photocatalytic decomposition of aqueous SA.

generated holes in the TiO_2 VB, producing •OH radicals that decomposed the organic compounds.

Several pieces of experimental evidence were used to confirm the hole-transfer mechanism for the $FeWO_4/TiO_2$ composite in this study. First, the generation of holes in TiO_2 VB was analyzed by monitoring the chemical reaction of the iodide ion (I^-), which is known as a hole scavenger. Generally, the I^-/I_3^-

dx.doi.org/10.1021/am502079x | ACS Appl. Mater. Interfaces 2014, 6, 9654−9663

Table 1. BET Surface Area, Degradation Rate Constants for IP (K_{IP}) and SA (K_{SA}), and Constants Per Unit Catalytic Surface Area (A) for Various Catalytic Systems

		2-Propanol, IP		Salicylic Acid, SA	
photocatalytic sample	BET surface area ($m^2\ g^{-1}$)	K_{IP} (h^{-1})	K_{IP}/A ($h^{-1}\ m^{-2}$)	K_{SA} (h^{-1})	K_{SA}/A ($h^{-1}\ m^{-2}$)
$FeWO_4$	15.0	0.034	0.283	0.003	0.025
TiO_2	191.3	0.021	0.014	0.003	0.002
N-TiO_2	62.1	0.211	0.425	0.021	0.042
3/97 $FeWO_4$/TiO_2	145.5	0.879	0.755	0.043	0.037
5/95 $FeWO_4$/TiO_2	140.3	1.314	1.171	0.053	0.047
7/93 $FeWO_4$/TiO_2	137.5	0.821	0.746	0.034	0.031
$FeWO_4$/TiO_2/CdS-0.5%	135.4	1.677	1.548	0.086	0.079
$FeWO_4$/TiO_2/CdS-1.0%	128.9	1.917	1.859	0.099	0.096
$FeWO_4$/TiO_2/CdS-1.5%	121.5	1.586	1.632	0.076	0.078

redox couple has been used as an electrolyte to mediate the charges in dye-sensitized solar cells, where the I^- ions accept holes from the HOMO of the dyes.[51,52] Hence, the I^- ions are expected to be oxidized to triiodide (I_3^-) by reacting with the holes generated in $FeWO_4$ or TiO_2 (see eq 9), because the redox potential of I^-/I_3^- is +0.536 V, which is much higher than the VB levels of $FeWO_4$ (+2.80 V) or TiO_2 (+2.70 V).[53]

$$3I^-(aq) + 2h^+ \rightarrow I_3^-(aq) \quad (9)$$

Fifty-milliliter (50-mL) samples of 0.01 M KI solution containing a suspension of $FeWO_4$, 5/95 $FeWO_4/TiO_2$, or TiO_2 (20 mg each) were irradiated for 2 h under visible light ($\lambda \geq 420$ nm). Then, the I_3^- formed in the solution was identified from its characteristic absorption peaks at 286 and 345 nm. Figure 6 shows the UV-vis absorption spectra of the KI solution, after the reaction with $FeWO_4$, $FeWO_4/TiO_2$, and TiO_2. The pure 0.01 M KI solution did not show any characteristic absorption peak after visible-light irradiation for 2 h. No characteristic I_3^- absorption peak was observed when the KI solution was irradiated in the presence of bare $FeWO_4$, indicating that bare $FeWO_4$ could not oxidize I^- under visible-light irradiation. For bare $FeWO_4$, electron and hole pairs were generated in its CB and VB, respectively, but the holes generated in $FeWO_4$ were not consumed in the formation of I_3^-, presumably because the electron−hole recombination was faster than the reaction between a hole and I^-. There was no characteristic I_3^- absorption peak when the KI solution was irradiated in the presence of bare TiO_2 under visible-light. However, under UV light irradiation, strong absorption peaks appeared at 286 and 345 nm, indicating the formation of a large quantity of I_3^-. Thus, the TiO_2 could not be excited by visible light, because of its wide E_g, but the holes that were generated in the VB by UV light could induce I_3^- formation. Notably, the characteristic I_3^- absorption peak was observed when the KI solution was irradiated in the presence of the 5/95 $FeWO_4/TiO_2$ (see Figure 6), clearly indicating that holes were generated in the TiO_2 VB. This result provides strong evidence that the visible-light photocatalytic activity of Type-B heterojunction systems originates from intersemiconductor hole transport.

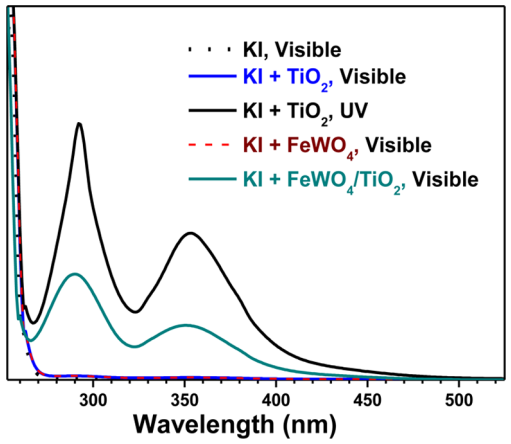

Figure 6. Ultraviolet−visible light (UV-vis) spectra of 0.01 M aqueous KI solution in the presence of different catalytic systems after visible-light ($\lambda \geq 420$ nm) or UV-light irradiation for 2 h.

Second, the presence of •OH radicals on the $FeWO_4/TiO_2$ surface during visible-light irradiation was also examined to provide further evidence of the hole-transfer mechanism, because holes in the TiO_2 VB spontaneously react with water or hydroxide to form •OH radicals, as shown in eqs 4 and 5.[54]

Equation 10 shows that •OH readily reacts with 1,4-terephthalic acid (TA) to form 2-hydroxy terephthalic acid

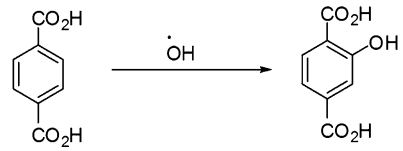

(10)

(TAOH), which emits a unique fluorescence peak at 426 nm by UV light excitation. This method has frequently been used to detect •OH in aqueous solution.[55] Herein, 20 mg of $FeWO_4$, TiO_2 or 5/95 $FeWO_4/TiO_2$ were suspended in 60 mL of an aqueous solution containing 0.01 M NaOH and 3 mM TA. The suspension was stirred in darkness for 30 min, and then irradiated for 1 h by visible light ($\lambda \geq 420$ nm). As shown in Figure 7, bare TiO_2, suspended in TA solution, did not show an

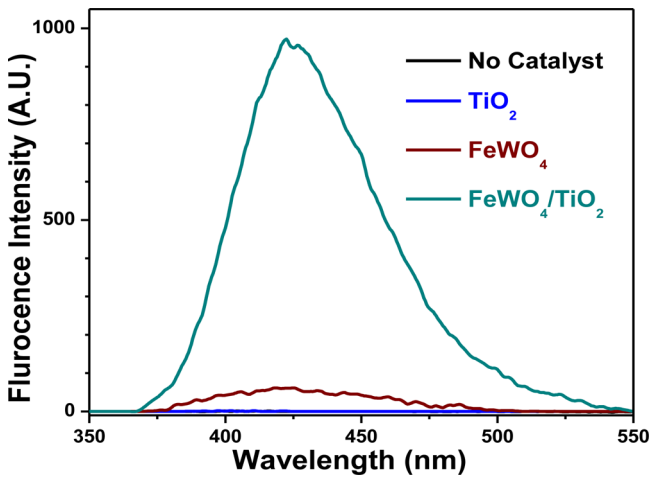

Figure 7. Fluorescence spectra of 3 mM TA solutions containing several catalytic systems after 1 h of irradiation with visible light; the wavelength of the excitation light used to obtain the fluorescence spectra was 312 nm.

dx.doi.org/10.1021/am502079x | ACS Appl. Mater. Interfaces 2014, 6, 9654−9663

appreciable fluorescence peak upon visible-light irradiation. Bare $FeWO_4$ exhibited a very low intensity peak, indicating that the photogenerated electron−hole pairs mostly recombined before the holes were utilized to form •OH. In contrast, the 5/95 $FeWO_4/TiO_2$ induced an intense fluorescence peak, whose intensity increased with the irradiation time. This result clearly indicates that holes formed at the TiO_2 side were transported from $FeWO_4$ by the intersemiconductor hole-transport mechanism.

A third experiment was performed, in which 0.10 g of bare $FeWO_4$ or 5/95 $FeWO_4/TiO_2$ were separately suspended in 20 mL of a 1.0 mM $HAuCl_4$ aqueous solution: each suspension was then irradiated by visible light ($\lambda \geq 420$ nm) for 1 h. $FeWO_4$ was excited by the irradiated visible-light in both samples. Considering that the standard reduction potential of Au^{3+}/Au is +1.498 V (vs NHE) and the CB level of $FeWO_4$ is +0.80 V (vs NHE), the generated electrons in $FeWO_4$ CB have sufficient chemical potential to reduce Au^{3+} to metallic Au, as shown in eq 11.

$$Au^{3+}(aq) + 3e^- \rightarrow Au(s) \qquad E_0 = +1.498\ V(vs\ NHE) \tag{11}$$

However, no metallic Au was deposited on the $FeWO_4$ surface, when bare $FeWO_4$ was used. This result indicates that the excited electrons on the $FeWO_4$ CB were not consumed in the Au^{3+} reduction reaction, because of the fast recombination of the electron−hole pairs. In contrast, a significant amount of metallic Au was deposited on the 5/95 $FeWO_4/TiO_2$. Figure 8

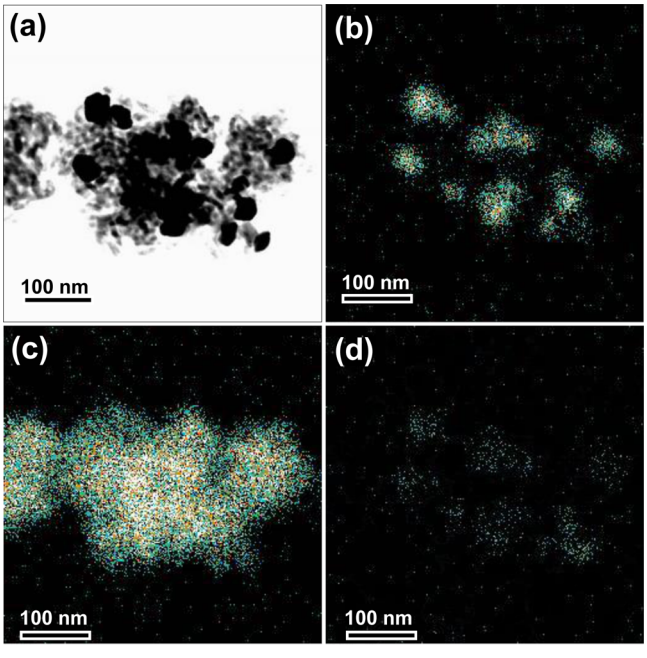

Figure 8. (a) TEM image of $FeWO_4/TiO_2$ after photodeposition of Au using visible-light and (b−d) EDX elemental mapping images to the corresponding area ((b) Au, (c) Ti, and (d) W).

shows a TEM image of the Au-deposited $FeWO_4/TiO_2$ and the corresponding elemental mapping images for Au, Ti, and W. The mapping image of Au in Figure 8b coincides with that of W in Figure 8d, clearly indicating that metallic Au was deposited only on the $FeWO_4$ side. The lifetime of the photoexcited electrons in $FeWO_4$ CB appears to have been significantly elongated by coupling with TiO_2, thereby inducing these electrons to participate in the Au^{3+} reduction reaction. Thus, the significantly longer lifetime resulted from the transfer of holes from the $FeWO_4$ VB to the TiO_2 VB. This result also supports the hole-transfer mechanism in this coupled system.

According to visible-light irradiation to the $FeWO_4/TiO_2$, the electron−hole pairs are formed in $FeWO_4$. These holes were found to be transferred to the TiO_2 VB and consumed in the oxidation reaction. For the catalytic reaction to continue, electrons in the $FeWO_4$ CB must be scavenged. Considering that the CB level of $FeWO_4$ (+0.80 V vs NHE) is significantly lower than the standard hydrogen potential, electrons cannot be directly transferred to oxygen molecules, as shown in eqs 1 and 2. Hence, we surmise that the electrons in the $FeWO_4$ CB are transported to the oxygen species through the multielectron process described in eqs 6 and 7.

Thus, far, several Type-B heterojunction structures have been developed, some of which, such as Ag_3PO_4/TiO_2 and Sb-doped SnO_2/TiO_2, have demonstrated visible-light photocatalytic activity that is comparable to that of N-TiO_2.[36,37] Herein, we found that the $FeWO_4/TiO_2$ system exhibited considerably higher catalytic activity than the previously reported systems. In designing efficient catalytic system, $FeWO_4$ offers the advantage of a narrow E_g that facilitates sufficient utilization of visible light and a suitable band location for efficient hole-transport. Moreover, because of its extended thermal stability, the annealing temperature can be elevated, thereby forming more crystallized TiO_2 and achieving tight binding between $FeWO_4$ and TiO_2. Fast hole diffusion and a low charge recombination rate are also required for the sensitizer, but these properties have not yet been reported for $FeWO_4$. Therefore, further investigation is necessary to understand the unique photocatalytic property of this system.

Herein to further increase the photocatalytic activity, a double heterojunction structure of $FeWO_4/TiO_2/CdS$ was formed by loading the CdS QD onto the surface of the 5/95 $FeWO_4/TiO_2$ composite. Scheme 1c describes the preparation strategy for the double heterojunction structure. Figure 9a

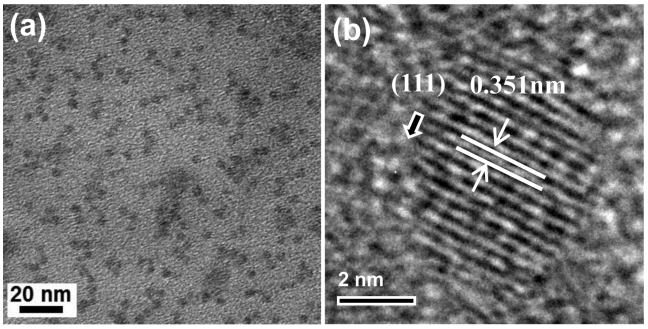

Figure 9. (a) TEM image of as-prepared MPA-capped CdS QD and (b) the corresponding high-resolution image.

shows TEM image of the CdS QD after surface modification by 3-mercaptopropionic acid (MPA). The as-prepared CdS QD was monodispersed with an average size of 6 nm. The high-resolution transmission electron microscopy (HRTEM) image in Figure 9b shows a CdS QD with uniform fringe patterns over its entire area. The fringe spacing of 0.351 nm was determined to be (111) plane of the CdS in the cubic $F\underline{4}3m$ space group.

Figure 10a shows a TEM image of the 1 wt % CdS-deposited $FeWO_4/TiO_2$, showing that the $FeWO_4$ NCs are located in the core and covered by TiO_2. Thus, the CdS QDs and $FeWO_4$

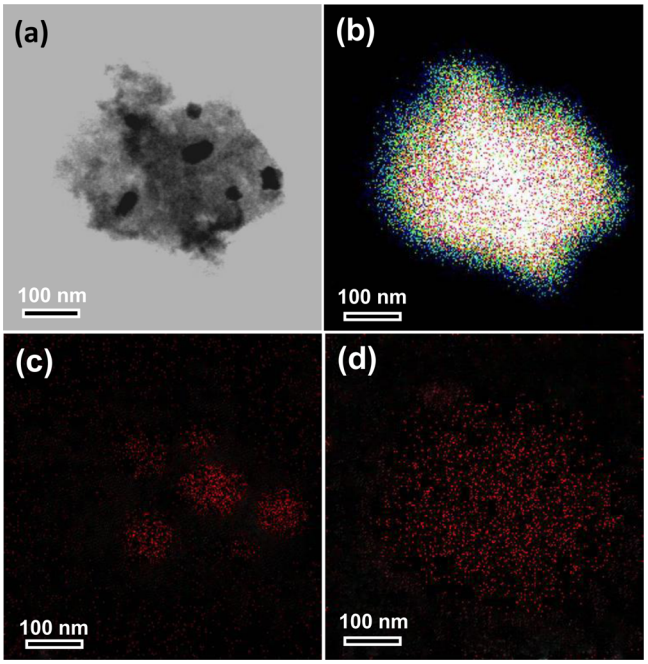

Figure 10. (a) TEM image of $FeWO_4/TiO_2/CdS$ (CdS:1 wt %) and (b–d) EDX elemental mapping images to the corresponding area: (b) Ti, (c) W, and (d) Cd.

NCs were spatially separated by the TiO_2 layer and did not contact each other. The EDX elemental mapping images were obtained for the 1-wt %-CdS-loaded $FeWO_4/TiO_2$ composite in the TEM image of Figure 10a. The Ti-mapping image shown in Figure 10b was very similar to the original image. Figure 10c shows the W-mapping image, indicating that $FeWO_4$ particles were embedded in the TiO_2 structure. Figure 10d shows the Cd elemental mapping image. The Cd signal was weak, but its overall image was similar to the original TEM image, indicating that the CdS QDs were uniformly distributed over the surface of the $FeWO_4/TiO_2$ composite. Thus, the CdS QDs were located on the TiO_2 surface, considering that the $FeWO_4$ surface was fully covered by TiO_2.

The photocatalytic activities of the $FeWO_4/TiO_2/CdS$ composites with different CdS compositions were evaluated by monitoring the decomposition of gaseous IP. The 1 wt % CdS-deposited $FeWO_4/TiO_2$ ($FeWO_4/TiO_2/CdS$-1%) exhibited the highest catalytic activity of all of the composites. The IP was completely removed in 100 min, whereas ~10% of the IP still remained for bare $FeWO_4/TiO_2$ after 2 h of visible-light irradiation (see Figure 11a). The amount of CO_2 evolved under visible-light irradiation was also monitored, as shown in Figure 11b. In 2 h, 37.9 ppm of CO_2 was evolved, which was 2.6 and 4.4 times greater than that evolved for bare $FeWO_4/TiO_2$ and N-TiO_2, respectively. In decomposing aqueous SA, $FeWO_4/TiO_2/CdS$-1% also exhibited greatly enhanced catalytic activity: the rate constant was 4.7 times greater than that of N-TiO_2, as listed in Table 1.

Scheme 1b outlines the photocatalytic mechanism of the $FeWO_4/TiO_2/CdS$ composite system. Under visible-light irradiation, both the $FeWO_4$ and CdS are excited. Then, the holes in $FeWO_4$ VB can move to TiO_2 VB,[32] while the photoexcited electrons in the CdS CB move to TiO_2 CB.[56−58] Thus, both electrons and holes can be generated in the CB and VB, respectively, of TiO_2. In general, the photoexcited electron/hole pairs in bare TiO_2 can quickly recombine.[59] In

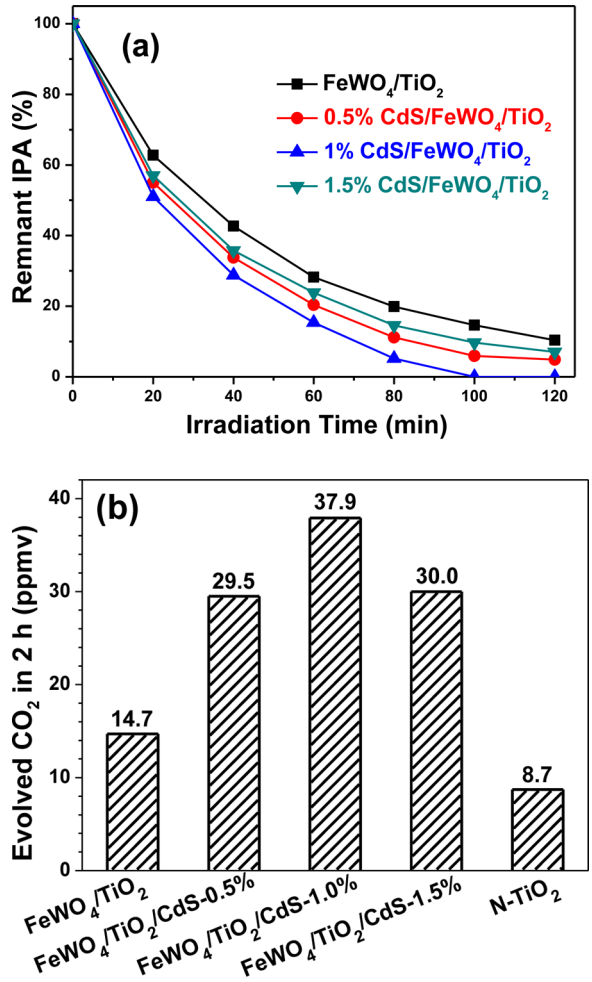

Figure 11. (a) Remnant IP concentration as a function of irradiation time and (b) amount of CO_2 evolved in 2 h during photocatalytic decomposition of gaseous IP under visible-light irradiation ($\lambda \geq 420$ nm). A $FeWO_4/TiO_2$ with a composition of 5/95 was used in all of the experiments.

this double heterojunction structure, however, the e^-–h^+ pairs generated in the TiO_2 have a relatively longer lifetime, because the electrons and holes are space-charge-separated.[36] That is, in the $FeWO_4/TiO_2/CdS$, $FeWO_4$ NCs are embedded in the core, and CdS QDs are loaded onto the surface of the TiO_2 structure. Thus, the electrons are generated in the region neighboring the CdS, whereas the holes are formed near the $FeWO_4$. Therefore, the space-charge-separated holes and electrons in the TiO_2 have more opportunities to participate in photocatalytic reactions.

In the present study, we demonstrated that a double-heterojunctioned $FeWO_4/TiO_2/CdS$ composite, generating both electrons and holes on the surface of TiO_2, exhibited considerably higher efficiencies in decomposing IP and evolving CO_2 than the $FeWO_4/TiO_2$ system, generating the holes only. This strongly suggests that both the holes in the TiO_2 VB and the electrons in the TiO_2 CB play important roles in the complete decomposition of organic compounds. As indicated in eqs 1 and 2, $HO_2\bullet$ can be formed from the electrons in the TiO_2 CB. Therefore, both $\bullet OH$ and $HO_2\bullet$ are key components in expediting the decomposition reactions.

dx.doi.org/10.1021/am502079x | ACS Appl. Mater. Interfaces 2014, 6, 9654−9663

CONCLUSIONS

5/95 $FeWO_4/TiO_2$ demonstrated remarkable photocatalytic activity under visible-light irradiation in removal of gaseous IP and in evolution of CO_2, whereas negligible activities were observed from bare $FeWO_4$ or TiO_2. The CO_2 evolved in 2 h was 14.7 ppmv, which was 1.7 times greater than that evolved using N-TiO_2. Thus, this notable catalytic performance originated from the intersemiconductor hole-transfer between the valence bands (VBs) of $FeWO_4$ and TiO_2. That is, the generated holes in the sensitizer VB are transported to that of TiO_2, thereby inducing the formation of •OH radicals. Evidence for hole transport between the sensitizer and TiO_2 were acquired from the following three experiments. First, it was found that I^- was converted to I_3^- by irradiating visible light in the presence of $FeWO_4/TiO_2$. Second, an aqueous suspension of $FeWO_4/TiO_2$ was found to convert 1,4-terephthalic acid (TA) to 2-hydroxy terephthalic acid (TAOH) in the presence of visible light. Third, metallic Au was only deposited on the $FeWO_4$ side of the $FeWO_4/TiO_2$ composite during the photodeposition of Au^{3+}. Notably, double-heterojunctioned $FeWO_4/TiO_2$/CdS demonstrated a remarkably enhanced activity in decomposing IP: the amount of CO_2 evolved was 37.9 ppmv after 2 h of irradiation, which was 2.6 and 4.4 times greater than that of bare $FeWO_4/TiO_2$ and typical N-TiO_2, respectively. The unusual catalytic property of this novel double-heterojunction structure resulted from the generation of both electrons and holes in the conduction band (CB) and VB, respectively, of TiO_2. Therefore, both the holes in the VB and the electrons in the CB play important roles in the complete decomposition of organic compounds.

AUTHOR INFORMATION

Corresponding Author

*E-mail: wanin@inha.ac.kr.

Author Contributions

†S.B. and S.B.R. contributed equally to this report.

Notes

The authors declare no competing financial interest.

ACKNOWLEDGMENTS

This work was supported by the Korea Center for Artificial Photosynthesis (KCAP) funded by the Minister of Science, ICT and Future Planning (MSIP) through the National Research Foundation of Korea (Project No. 2009-0093883), and the National Research Foundation of Korea (Project No. 2011-0002995).

REFERENCES

(1) Fujishma, A.; Honda, K. Electrochemical Photolysis of Water at a Semiconductor Electrode. *Nature* **1972**, *238*, 37−38.

(2) Hoffmann, M. R.; Martin, S. T.; Choi, W.; Bahnemann, D. W. Environmental Applications of Semiconductor Photocatalysis. *Chem. Rev.* **1995**, *95*, 69−96.

(3) Anpo, M.; Takeuchi, M. The Design and Development of Highly Reactive Titanium Oxide Photocatalysts Operating under Visible Light Irradiation. *J. Catal.* **2003**, *216*, 505−516.

(4) Thompson, T. L.; Yates, J. T., Jr. Surface Science Studies of the Photoactivation of TiO_2—New Photochemical Processes. *Chem. Rev.* **2006**, *106*, 4428−4453.

(5) Ou, Y.; Lin, J.; Fang, S.; Liao, D. Study on the Preparation of Ultrafine Mesoporous TiO_2 with Controllable Crystalline Phase and Its Photocatalytic Activities. *Catal. Commun.* **2007**, *8*, 936−940.

(6) Kubacka, A.; Fernandez-García, M.; Colon, G. Advanced Nanoarchitectures for Solar Photocatalytic Applications. *Chem. Rev.* **2012**, *112*, 1555−1614.

(7) Burda, C.; Lou, Y.; Chen, X.; Samia, A. C. S.; Stout, J.; Gole, J. L. Enhanced Nitrogen Doping in TiO_2 Nanoparticles. *Nano Lett.* **2003**, *3*, 1049−1051.

(8) Justica, I.; Ordejon, P.; Cano, G.; Mozos, J. L.; Frazedas, J.; Battiston, G. A.; Gerbasi, R.; Figueras, A. Design of Self-Doped Titanium Oxide Thin Films for Efficient Visible-Light Photocatalysis. *Adv. Mater.* **2002**, *14*, 1399−1402.

(9) Yu, H.; Irie, H.; Shimodaira, Y.; Hosogi, Y.; Kuroda, Y.; Miyauchi, M.; Hashimoto, K. An Efficient Visible-Light-Sensitive Fe(III)-Grafted TiO_2 Photocatalyst. *J. Phys. Chem. C* **2010**, *114*, 16481−16487.

(10) Sakthivel, S.; Kisch, H. Photocatalytic and Photoelectrochemical Properties of Nitrogen-Doped Titanium Dioxide. *ChemPhysChem* **2003**, *4*, 487−490.

(11) Zhao, W.; Ma, W.; Chen, C.; Zhao, J.; Shuai, Z. Efficient Degradation of Toxic Organic Pollutants with $Ni_2O_3/TiO_{2-x}B_x$ under Visible Irradiation. *J. Am. Chem. Soc.* **2004**, *126*, 4782−4783.

(12) Borgarello, E.; Kiwi, J.; Gratzel, M.; Pelizzetti, E.; Visca, M. Visible Light Induced Water Cleavage in Colloidal Solutions of Chromium-Doped Titanium Dioxide Particles. *J. Am. Chem. Soc.* **1982**, *104*, 2996−3002.

(13) Nakhatea, G. G.; Nikama, V. S.; Kanadea, K. G.; Arbujb, S.; Kaleb, B. B.; Baegc, J. O. Hydrothermally Derived Nanosized Ni-Doped TiO_2: A Visible Light Driven Photocatalyst for Methylene Blue Degradation. *Mater. Chem. Phys.* **2010**, *124*, 976−981.

(14) Klosek, S.; Raftery, D. Visible Light Driven V-Doped TiO_2 Photocatalyst and Its Photooxidation of Ethanol. *J. Phys. Chem. B* **2001**, *105*, 2815−2819.

(15) Choi, W.; Termin, A.; Hoffmann, M. R. The Role of Metal Ion Dopants in Quantum-Sized TiO_2: Correlation between Photoreactivity and Charge Carrier Recombination Dynamics. *J. Phys. Chem.* **1994**, *98*, 13669−13679.

(16) Bouras, P.; Stathatos, E.; Lianos, P. Pure versus Metal-Ion-Doped Nanocrystalline Titania for Photocatalysis. *Appl. Catal., B* **2007**, *73*, 51−59.

(17) Peng, B.; Meng, X.; Tang, F.; Ren, X.; Chen, D.; Ren, J. General Synthesis and Optical Properties of Monodisperse Multifunctional Metal-Ion-Doped TiO_2 Hollow Particles. *J. Phys. Chem. C* **2009**, *113*, 20240−20245.

(18) Asahi, R.; Morikawa, T.; Ohwaki, T.; Aoki, K.; Taga, Y. Visible-Light Photocatalysis in Nitrogen-Doped Titanium Oxides. *Science* **2001**, *293*, 269−271.

(19) Tachikawa, T.; Tojo, S.; Kawai, K.; Endo, M.; Fujitsuka, M.; Ohno, T.; Nishijima, K.; Miyamoto, Z.; Majima, T. Photocatalytic Oxidation Reactivity of Holes in the Sulfur- and Carbon-Doped TiO_2 Powders Studied by Time-Resolved Diffuse Reflectance Spectroscopy. *J. Phys. Chem. B* **2004**, *108*, 19299−19306.

(20) Dong, F.; Wang, H.; Wu, Z. One-Step "Green" Synthetic Approach for Mesoporous C-Doped Titanium Dioxide with Efficient Visible Light Photocatalytic Activity. *J. Phys. Chem. C* **2009**, *113*, 16717−16723.

(21) Yu, J. C.; Ho, W.; Yu, J.; Yip, H.; Wong, P. K.; Zhao, J. Efficient Visible-Light-Induced Photocatalytic Disinfection on Sulfur-Doped Nanocrystalline Titania. J. *Environ. Sci. Technol.* **2005**, *39*, 1175−1179.

(22) Stengl, V.; Houskova, V.; Bakardjieva, S.; Murafa, N. Photocatalytic Activity of Boron -Modified Titania under UV and Visible-Light Illumination. *ACS Appl. Mater. Interfaces* **2010**, *2*, 575−580.

(23) Liu, G.; Wang, L.; Yang, H. G.; Cheng, H. M.; Lu, G. Q. Titania-Based Photocatalysts—Crystal Growth, Doping and Heterostructuring. *J. Mater. Chem.* **2010**, *20*, 831−843.

(24) Liu, D.; Kamat, P. V. Electrochemical rectification in CdSe + TiO_2 Coupled Semiconductor Films. *J. Electroanal. Chem.* **1993**, *347*, 451−456.

(25) Spanhel, L.; Weller, H.; Henglein, A. Photochemistry of Semiconductor Colloids. 22. Electron Injection from Illuminated CdS

into Attached TiO_2 and ZnO Particles. *J. Am. Chem. Soc.* **1987**, *109*, 6632−6635.
(26) Yu, X.; Wu, Q.; Jiang, S.; Guo, Y. Nanoscale ZnS/TiO_2 composites: Preparation, Characterization, and Visible-Light Photocatalytic Activity. *Mater. Charact.* **2006**, *57*, 333−341.
(27) Kim, J. C.; Choi, J. K.; Lee, Y. B.; Hong, J. H.; Lee, J. I.; Yang, J. W.; Lee, W. I.; Hur, N. H. Enhanced Photocatalytic Activity in Composites of TiO_2 Nanotubes and CdS Nanoparticles. *Chem. Commun.* **2006**, 5024−5026.
(28) Bessekhouad, Y.; Chaoui, N.; Trzpit, M.; Ghazzal, N.; Robert, D.; Weber, J. V. UV−Vis versus Visible Degradation of Acid Orange II in a Coupled CdS/TiO_2 Semiconductors Suspension. *Photochem. Photobiol. A* **2006**, *183*, 218−224.
(29) Agrios, A. G.; Pichat, P. State of the Art and Perspectives on Materials and Applications of Photocatalysis over TiO_2. *J. Appl. Electrochem.* **2005**, *35*, 655−663.
(30) Gaya, U. I.; Abdullah, A. H. Heterogeneous Photocatalytic Degradation of Organic Contaminants over Titanium Dioxide: A Review of Fundamentals, Progress and Problems. *J. Photochem. Photobiol. C* **2008**, *9*, 1−12.
(31) Gnaser, H.; Savina, M. R.; Chalaway, W. F.; Tripa, C. E.; Veryovkin, I. V.; Pellin, M. J. Photocatalytic Degradation of Methylene Blue on Nanocrystalline TiO_2: Surface Mass Spectrometry of Reaction Intermediates. *Int. J. Mass Spectrom.* **2005**, *245*, 61−67.
(32) Rawal, S. B.; Bera, S.; Lee, D.; Jang, D. J.; Lee, W. I. Design of Visible-Light Photocatalysts by Coupling of Narrow Bandgap Semiconductors and TiO_2: Effect of Their Relative Energy Band Positions on the Photocatalytic Efficiency. *Catal. Sci. Technol.* **2013**, *3*, 1822−1830.
(33) Leghari, S. A. K.; Sajjad, S.; Chen, F.; Zhang, J. WO_3/TiO_2 Composite with Morphology Change via Hydrothermal Template-Free Route as an Efficient Visible Light Photocatalyst. *Chem. Eng. J.* **2011**, *166*, 906−915.
(34) Kim, Y. J.; Gao, B.; Han, S. Y.; Jung, M. H.; Chakraborty, A. K.; Ko, T. G.; Lee, C. M.; Lee, W. I. Heterojunction of $FeTiO_3$ Nanodisc and TiO_2 Nanoparticle for a Novel Visible Light Photocatalyst. *J. Phys. Chem. C* **2009**, *113*, 19179−19184.
(35) Bian, Z.; Zhu, J.; Wang, S.; Cao, Y.; Qian, X.; Li, H. Self-Assembly of Active Bi_2O_3/TiO_2 Visible Photocatalyst with Ordered Mesoporous Structure and Highly Crystallized Anatase. *J. Phys. Chem. C* **2008**, *112*, 6258−6262.
(36) Rawal, S. B.; Chakraborty, A. K.; Kim, Y. J.; Kim, H. J.; Lee, W. I. Double-Heterojunction Structure of $Sb_xSn_{1-x}O_2/TiO_2/CdSe$ for Efficient Decomposition of Gaseous 2-propanol under Visible-Light Irradiation. *RSC Adv.* **2012**, *2*, 622−630.
(37) Rawal, S. B.; Sang, S. D.; Lee, W. I. Novel Ag_3PO_4/TiO_2 Composites for Efficient Decomposition of Gaseous 2-propanol under Visible-Light Irradiation. *Catal. Commun.* **2012**, *17*, 131−135.
(38) Rawal, S. B.; Bera, S.; Lee, W. I. Visible-Light Photocatalytic Properties of $W_{18}O_{49}/TiO_2$ and WO_3/TiO_2 Heterocomposites. *Catal. Lett.* **2012**, *142*, 1482−1488.
(39) Anderson, A. B.; Albu, T. V. Ab Initio Determination of Reversible Potentials and Activation Energies for Outer-Sphere Oxygen Reduction to Water and the Reverse Oxidation Reaction. *J. Am. Chem. Soc.* **1999**, *121*, 11855−11863.
(40) Irie, H.; Miura, S.; Kamiya, K.; Hashimoto, K. Efficient Visible Light-Sensitive Photocatalysts: Grafting Cu(II) Ions onto TiO_2 and WO_3 Photocatalysts. *Chem. Phys. Lett.* **2008**, *457*, 202−205.
(41) Rajagopala, S.; Nataraja, D.; Khyzhunb, O. Y.; Djaouedc, Y.; Robichaudc, J.; Mangalaraj, D. Hydrothermal Synthesis and Electronic Properties of $FeWO_4$ and $CoWO_4$ Nanostructures. *J. Alloys Compd.* **2010**, *493*, 340−345.
(42) Shim, H. W.; Cho, I. S.; Hong, K. S.; Cho, W. I.; Kim, D. W. Li Electroactivity of Iron (II) Tungstate Nanorods. *Nanotechnol.* **2010**, *21*, 465602−465608.
(43) Yu, F.; Cao, L.; Huang, J.; Wu, J. Effects of pH on the Micro Structures and Optical Property of $FeWO_4$ Nanocrystallites Prepared via Hydrothermal Method. *Ceram. Int.* **2013**, *39*, 4133−4138.
(44) Zhang, J.; Wang, Y.; Li, S.; Wang, X.; Huang, F.; Xie, A.; Shen, Y. Controlled Synthesis, Growth Mechanism and Optical Properties of $FeWO_4$ Hierarchical Microstructures. *Cryst. Eng. Commun.* **2011**, *13*, 5744−5750.
(45) Rajagopala, S.; Bekenevb, V. L.; Nataraja, D.; Mangalarajc, D.; Khyzhunb, O. Y. Electronic Structure of $FeWO_4$ and $CoWO_4$ Tungstates: First-Principles FP-LAPW Calculations and X-ray Spectroscopy Studies. *J. Alloys Compd.* **2010**, *496*, 61−68.
(46) Lacomba-Perales, R.; Ruiz-Fuertes, J.; Errandonea, D.; Martinez-Garcia, D.; Segura, A. Optical Absorption of Divalent Metal Tungstates: Correlation between the Band-Gap Energy and the Cation Ionic Radius. *Europhys. Lett.* **2008**, *83*, 37002−37007.
(47) Irie, H.; Watanabe, Y.; Hashimoto, K. Nitrogen-Concentration Dependence on Photocatalytic Activity of $TiO_{2-x}N_x$ Powders. *J. Phys. Chem. B* **2003**, *107*, 5483−5486.
(48) Leschkies, K. S.; Divakar, R.; Basu, J.; Pommer, E. E.; Boercker, J. E.; Carter, C. B.; Kortshagen, U. R.; Norris, D. J.; Aydil, E. S. Photosensitization of ZnO Nanowires with CdSe Quantum Dots for Photovoltaic Devices. *Nano Lett.* **2007**, *7*, 1793−1798.
(49) Kennedy, J. H.; Frese, K. W., Jr. Flatband Potentials and Donor Densities of Polycrystalline α-Fe_2O_3 Determined from Mott−Schottky Plots. *J. Electrochem. Soc.* **1978**, *125*, 723−726.
(50) Ejima, T.; Banse, T.; Takatsuka, H.; Kondo, Y.; Ishino, M.; Kimura, N.; Watanabe, M.; Matsubara, I. Microscopic Optical and Photoelectron Measurements of MWO_4 (M = Mn, Fe, and Ni). *J. Lumin.* **2006**, *119−120*, 59−63.
(51) Grätzel, M. Photoelectrochemical Cells. *Nature* **2001**, *414*, 338−344.
(52) Wang, M.; Chamberland, N.; Breau, L.; Moser, J. E.; Baker, R. H.; Marsan, B.; Zakeeruddin, S. M.; Grätzel, M. An Organic Redox Electrolyte to Rival Triiodide/Iodide in Dye-Sensitized Solar Cells. *Nat. Chem.* **2010**, *2*, 385−389.
(53) Serpone, N.; Maruthamuthu, P.; Pichat, P.; Pelizzetti, E.; Hidaka, H. Exploiting the Interparticle Electron Transfer Process in the Photocatalysed Oxidation of Phenol, 2-chlorophenol and Pentachlorophenol: Chemical Evidence for Electron and Hole Transfer between Coupled Semiconductors. *J. Photochem. Photobiol., A* **1995**, *85*, 247−255.
(54) Ishibashi, K.; Fujishima, A.; Watanabe, T.; Hashimoto, K. Quantum Yields of Active Oxidative Species Formed on TiO_2 Photocatalyst. *J. Photochem. Photobiol., A* **2000**, *134*, 139−142.
(55) Huang, H.; Li, D.; Lin, Q.; Zhang, W.; Shao, Y.; Chen, Y.; Sun, M.; Fu, X. Efficient Degradation of Benzene over $LaVO_4/TiO_2$ Nanocrystalline Heterojunction Photocatalyst under Visible Light Irradiation. *Environ. Sci. Technol.* **2009**, *43*, 4164−4168.
(56) Serpone, N.; Borgarello, E.; Grätzel, M. Visible Light Induced Generation of Hydrogen from H_2S in Mixed Semiconductor Dispersions; Improved Efficiency through Inter-Particle Electron Transfer. *J. Chem. Soc., Chem. Commun.* **1984**, 342−244.
(57) Sun, W. T.; Yu, Y.; Pan, H. Y.; Gao, X. F.; Chen, Q.; Peng, L. M. CdS Quantum Dots Sensitized TiO_2 Nanotube-Array Photoelectrodes. *J. Am. Chem. Soc.* **2008**, *130*, 1124−1125.
(58) Park, H.; Choi, W.; Hoffmann, M. R. Effects of the Preparation Method of the Ternary $CdS/TiO_2/Pt$ Hybrid Photocatalysts on Visible Light-Induced Hydrogen Production. *J. Mater. Chem.* **2008**, *18*, 2379−2385.
(59) Rothenberger, G.; Moser, J.; Grätzel, M.; Serpone, N.; Sharma, D. K. Charge Carrier Trapping and Recombination Dynamics in Small Semiconductor Particles. *J. Am. Chem. Soc.* **1985**, *107*, 8054−8059.